# A novel multiple training-scale dynamic adaptive cuckoo search optimized long short-term memory neural network and multi-dimensional health indicators acquisition strategy for whole life cycle health evaluation of lithium-ion batteries.

REN, P., WANG, S., CHEN, X., ZHOU, H., FERNANDEZ, C. and STROE, D.-I.

2022

# A novel multiple training-scale dynamic adaptive cuckoo search optimized long short-term memory neural network and multi-dimensional health indicators acquisition strategy for whole life cycle health evaluation of lithium-ion batteries

***Pu Ren*[1,2], *Shunli Wang*[1,2*], *Xianpei Chen*[1,2], *Heng Zhou*[1,2], *Carlos Fernandez*[4], *Daniel-Ioan Stroe*[3]**

([1]School of Information Engineering, Southwest University of Science and Technology, Mianyang 621010, China; [2]College of Electrical Engineering, Sichuan University, Chengdu 610065, China; [3]Department of Energy Technology, Aalborg University, Pontoppidanstraede 111 9220 Aalborg East, Denmark; [4]School of Pharmacy and Life Sciences, Robert Gordon University, Aberdeen AB10-7GJ, UK.)

## Highlights

- A dynamic adaptive cuckoo search optimized long short-term memory neural network is proposed for the state of health estimation.
- Nine features highly divided into measured and calculated health indicators are extracted.
- The proposed method is validated with seven groups of data from CALCE and NASA.

**Abstract:** State of health evaluation of lithium-ion batteries has become a significant research direction in related fields attributed to the crucial impact on the reliability and safety of electric vehicles. In this research, a dynamic adaptive cuckoo search optimized long short-term memory neural network algorithm is proposed. The aging mechanism of the battery is described effectively by extracting and selecting high correlation health indicators including voltage, current, charging time, etc. A dynamic adaptive strategy is introduced to the cuckoo search algorithm to stabilize the step size and improve the global search ability. The hyperparameter optimization and noise filtering problems of the long short-term memory model are solved and the accuracy of the algorithm is improved by taking advantage of the

established dynamic adaptive cuckoo search algorithm. The accuracy and effectiveness of the proposed method are verified based on the seven groups of battery aging datasets from the National Aeronautics and Space Administration and the University of Maryland. Compared with the long short-term memory and convolutional neural network long short-term memory, the mean absolute error of the results obtained by the proposed algorithm is kept under 2%, the root mean square error is less than 3%, and the average absolute percentage error is less than 3%. The results indicate the algorithm has better fitting performance, stronger robustness, and generality.

**Keywords:** state of health; dynamic adaptive cuckoo search optimized long short-term memory neural network; health characteristic indexes; global search ability; battery aging

## 1. Introduction

The development of new energy vehicle technology is a strategic measure to alleviate the world energy crisis and achieve the goal of carbon neutrality [1-3]. Lithium-ion battery (LIB) gradually turns into the most popular type of power battery for new energy vehicles due to its high energy density [4], long cycle life [5], and low self-discharge rate [6]. However, the performance of lithium-ion batteries may decrease with the irreversible degradation of the internal electrochemical components during the application, which is known as battery aging [7]. Battery aging brings the safety and reliability problems of batteries, leading to the degradation of electrical equipment performance or system failure, and even causing fire or explosion problems, greatly affecting the further industrial application of lithium-ion batteries [8]. In order to ensure the safety and reliability of batteries, the health management technology of lithium-ion batteries has been developed continuously [9]. The state of health (SOH) of a battery is an important evaluation index of battery health management, which reflects the health status of the battery during operation [10]. It is of great significance to accurately evaluate the SOH of power batteries for new energy vehicles in terms of energy refinement management, maintenance [11], safety warning, and residual value evaluation of successive utilization of power batteries.

SOH is originally proposed to evaluate the degree of aging of batteries relative to new ones [12]. The aging of the battery is attributed to the complex electrochemical reaction inside the battery, and its direct impact on the battery performance is the decrease of the capacity and the increase of

the internal resistance [13]. Therefore, the industry generally takes advantage of capacity and internal resistance to define the SOH of a battery [14]. Under normal circumstances, when the actual capacity of the electric vehicle battery drops to 80% of the rated capacity or the internal resistance increases to 2 times the original, it is deemed to enter the end-of-life (EOL) state [15]. For hybrid electric vehicles (HEVs), battery SOH is primarily measured by internal resistance, as power capability is more significant in this application. In contrast, for pure electric vehicles (PEVs), battery SOH is usually evaluated based on actual capacity due to the importance of energy capability in this application [16]. Compared with the internal resistance of the battery that can be directly calculated through the pulse condition, the degradation process of the battery capacity is very complex and is greatly affected by many factors such as temperature, current rate, historical aging path, etc., and in the case of incomplete discharge or charge cycles, the capacity cannot be measured online at all [17]. Therefore, how to use artificial intelligence technology to develop an effective prediction model or method theory so as to achieve an accurate prediction of capacity degradation trend, so as to achieve early failure detection of lithium-ion batteries, is more challenging and attracts the attention of many researchers in this field [18]. Hence, this paper focuses on capacity-based SOH estimation to conduct a series of studies.

At present, based on differences in principles and structures, SOH estimation methods are mainly divided into three categories: experimental analysis, model-based, and data-driven [19]. The experimental analysis method evaluates battery SOH by directly measuring battery capacity, internal resistance, impedance spectrum, and other characteristic parameters [20], or on the basis of direct measurement, some characteristic quantities that can reflect battery capacity or internal resistance decline are selected, and battery aging status is indirectly reflected through the change of characteristic parameters [21], so as to evaluate battery SOH. The experimental analysis method includes the Coulomb counting method, open circuit voltage method, impedance spectroscopy [22], etc. Huang et al. [23] propose a comprehensive optimization framework for Li-ion battery SOH estimation with the Local Coulomb Counting Curve (LCCC). Bian et al. [8] develop a novel OCV model to extract the OCV curve and the features of

interest (FOIs) associated with SOH. Ouyang et al. [24] establish the Gaussian linear models based on parameters of six commonly used open-circuit-voltage models to estimate SOH. Jiang et al. [25] investigate a systematic comparative study of three categories of features extracted from battery electrochemical impedance spectroscopy (EIS) in SOH estimation. However, the experimental conditions of the experimental method are greatly affected by the external environment, and experimental measurement errors are unavoidable [26], which makes it difficult to apply in practical applications. The model-based method extracts corresponding models according to various electrochemical reactions in the battery and the prior knowledge of the life cycle and physical and chemical reaction laws are taken advantage of to realize the evaluation of SOH [27]. Electrochemical models (EMs) or equivalent circuit models (ECMs) are the most commonly used models [28]. Xu et al. [29] propose a minimalist electrochemical model to relate SOH to capacity fading due to the irreversible loss of Li. Gao et al. [15] develop a scheme using the reduced-order electrochemical model and the dual nonlinear filters for the reliable co-estimations of cell SOC and SOH. Liu et al. [30] propose an autoregressive equivalent circuit model (AR-ECM) to realize the joint estimation method for the SOH, state of charge (SOC), and state of power (SOP) of batteries. Sakile et al. [31] propose an adaptive nonlinear observer (ANO) for SOH estimation based on a first-order resistor-capacitor (RC) electrical equivalent circuit model. However, the EMs need to solve complex partial differential equations, which increases the burden of the battery management system [32], and the ECMs are difficult to accurately reflect the battery decay process attributed to the influence of objective factors [33], and the robustness and accuracy of the models lack. In contrast, data-driven methods gain increasing attention from academia and industry [34], and when sufficient data are available, models for SOH estimation with high accuracy for specific applications can be easily built.

The data-driven method does not require physical insight into aging dynamics by using large amounts of historical battery measurements but takes advantage of machine learning methods to establish relevant models [35]. Therefore, the method is more flexible and diverse and has better application prospects. The core of the data-driven method lies in the selection and

processing of data [36], and the key reflects in extracting features that are highly correlated with the target output and establishing the relationship between feature parameters and SOH [37]. In recent years, data processing methods are enriched continuously, and algorithms such as neural network (NN), support vector regression (SVR), relevance vector machine (RVM), Gaussian process regression (GPR), Bayesian model (BM), random forest (RF), and autoencoder (AE) have appeared [38], which show the excellent effect in the evaluation of SOH. Lin et al. [39] propose a novel SOH estimation method based on the fusion of the simulated annealing (SA) algorithm and SVR. Wu et al. [40] establish a synergetic method with the help of the genetic algorithm (GA) and the support vector regression (SVR) for SOH estimation. Lyu et al. [41] develop a hybrid kernel function relevance vector machine (HKRVM) optimized model for battery prognostics and health management. Sun et al. [42] present an optimized multiple kernel relevance vector machine (MKRVM). Deng et al. [43] propose a method based on the random partial charging process and sparse Gaussian process regression. Li et al. [44] build a closed-loop battery capacity estimation framework, Gaussian process regression, and multi-output Gaussian process regression for constructing battery dynamic state-space function. Dong et al. [45] present a probabilistic method for the battery degradation modeling and health prognosis based on the features extracted from the charging process using the dynamic Bayesian network (DBN). Haris et al. [46] propose a novel combination of deep learning algorithm-Deep Belief Network (DBN) with Bayesian Optimization and HyperBand (BOHB) to predict the RUL. Mawonou et al. [47] propose a data-driven battery aging prediction using the random forest (RF) algorithm based on actual users' behavior and ambient conditions. Xu et al. [48] design a novel physics-informed machine learning prognostic model named PIDDA based on an autoencoder. Among them, the neural network algorithm has achieved the most outstanding results and has become the most common data-driven algorithm.

A neural network algorithm is to simulate the thinking process of the human brain in mathematical form, the network formed by connecting neurons in a certain way through a large number of data to train the threshold and weight between neurons to get the prediction model [49]. Attribute to its high applicability in complex nonlinear modeling

problems with multi-correlated features, strong self-learning ability, and high prediction accuracy, the NN algorithm has become a mainstream data-driven technology and has achieved extensive results in the field of lithium-ion battery health management [50]. According to the differences in structure and working principle, common neural networks can be divided into three kinds including feedforward neural networks (FNN), convolutional neural networks (CNN), and recurrent neural networks (RNN) [51]. Yang et al. [52] utilize the convolutional neural network (CNN) to extract indicators for both SOH and changes in SOH (Delta SOH) between two successive charge/discharge cycles. Ma et al. [53] propose a transfer learning-based method for personalized SOH estimation of a new battery. A CNN combined with an improved domain adaptation method was used to construct a SOH estimation model, where the CNN was taken advantage of to automatically extract features from raw charging voltage trajectories. Che et al. [54] establish an improved dynamic recurrent neural network (DRNN) with the ability of dynamic mapping was established, which was more suitable than the static network for estimating the batteries' state with strongly nonlinear and dynamic behaviors. Chen et al. [55] develop a hybrid data science model based on empirical mode decomposition (EMD), grey relational analysis (GRA), and deep recurrent neural networks for the RUL prediction of lithium-ion batteries. As an improved type of RNN not only considering the influence of the historical aging path on battery health, but also the long short-term memory (LSTM) neural network overcomes the problem of gradient disappearance or explosion in the common RNN, and discards redundant information while memorizing long-term useful information [56]. This kind of algorithm and the improved forms become an important research direction in the field of neural network algorithms in recent years.

SOH estimation can be defined as time series processing problems, and LSTM neural network has obvious advantages in processing time series data [57]. Therefore, it is logical to use LSTM NN to monitor the health status of lithium-ion batteries. In recent years, a large number of related research results also proves the advantages of LSTM in dealing with the health management of lithium-ion batteries [19, 58]. Shu et al. [59] incorporate the LSTM network and transfer learning (TL) with the fine-tuning strategy for SOH prediction with

partial training data. Gong et al. [60] propose a data-driven estimation method based on the improved LSTM, where the network topology was estimated by the particle swarm optimization (PSO) algorithm. Wang et al. [61] establish a bidirectional long short-term memory with attention mechanism (Bi-LSTM-AM) model to predict online RUL by continuously updating the model parameters. Ma et al. [62] propose a novel differential evolution grey wolf optimization long short-term memory (DEGWO-LSTM) and health indicators (HIs) extraction from the charging-discharging process, and the method was verified based on the dataset of the battery from the National Aeronautics and Space Administration (NASA) and Massachusetts Institute of Technology (MIT). Heinrich et al. [63] present a LSTM-based neural network that learned the electrical behavior of an automotive battery cell based on in-vehicle driving data. This LSTM model was then taken advantage of to simulate the electric response during capacity testing, incremental capacity analysis, and peak-power testing. These studies show that LSTM does have great potential and application prospects in battery state of health estimation. However, although the LSTM neural network algorithm can be well utilized for the health monitoring of lithium-ion batteries, there are still three issues worth considering.

(1) Since a single LSTM algorithm cannot guarantee the accuracy, existing data-driven models often combine the LSTM algorithm with other neural networks or strategies to obtain better prediction results. However, this increases the complexity of the system, and there is no corresponding denoising method combined with the neural network model, resulting in a large deviation of the results.

(2) In the process of extracting characteristic variables of lithium-ion batteries, most studies often only consider one type of information system [57]. There is a certain internal relationship between variables, which may affect each other. At the same time, there is also a lack of direct description of the degree to which health characteristics are related to the state of health by mathematical index, but focus on direct selection based on experience. This leads to the limitation of aging information mining, which in turn affects the accuracy of later modeling.

(3) When a SOH estimation model based on the LSTM neural network algorithm is established, the selection of some

hyperparameters needs to be considered. The number of hidden neurons and the initial learning rate are the core hyperparameters, and the adaptive control of the two parameters is the important content to avoid overfitting, strengthen the convergence speed and improve the accuracy of the LSTM model. However, most current research ignores this important problem, resulting in a large error in the final estimation result.

This study attempts to address the above questions. The contributions are summarized accordingly as follows. Firstly, a SOH estimation strategy based on dynamic adaptive cuckoo search long short-term memory (DACS_LSTM) neural network algorithm is proposed by combining filtering algorithm and neural network methods. The combination of the LSTM algorithm and DACS algorithm has low overall complexity, and the effect of noise can be effectively reduced after filtering by the DACS algorithm. Secondly, multi-dimensional measured and calculated HIs are taken advantage of to describe the aging process of the battery, and the association between selected HIs and SOH is evaluated at the mathematical levels. The factors affecting the battery SOH are taken into account comprehensively. Thirdly, the improved DACS algorithm can effectively improve the search performance and the global optimization ability of the algorithm, which optimize the hyperparameters including the number of hidden neurons and the initial learning rate of the established prediction model built by long short-term neural network algorithm for the state of health estimation effectively. And the effect of SOH estimation of the DACS_LSTM algorithm is verified in seven groups of data from NASA and Computer Aided Life Cycle Engineering Center (CALCE).

The overall structure of this paper is as follows. Section 2 introduces the estimation theory of SOH and the establishment process of the DACS_LSTM algorithm. Section 3 presents the quantitative analysis of datasets, the extraction of HIs, and the overall framework of the state of health estimation. Section 4 describes the results of SOH estimation under four datasets and the comparison of algorithm performance. And the conclusions are given in Section 5.

## 2. SOH estimation theory and algorithm establishment

### 2.1 SOH estimation analysis

Attributed to the reason exposited in Section 1, this paper characterizes the state of health from the perspective of capacity decay. SOH can be defined as the ratio of

the actual capacity to the rated capacity of the battery [64], as shown in Eq. (1).

$$SOH = \frac{C_{act}}{C_{rat}} * 100\% \quad (1)$$

Wherein, $C_{act}$ stands for the actual capacity of the battery at the current time, and $C_{rat}$ represents the rated capacity of the battery. The rated capacity of the battery tested on the dataset used in this paper is known, hence the ultimate goal of this research is to obtain the actual capacity.

### 2.2 LSTM neural network algorithm dissection

There is an obvious iterative relationship in the process of complete charge and discharge of the lithium-ion battery, that is, the data of this cycle is not only related to the current experimental conditions but also affected by the last cycle. To clarify this kind of relationship between the current and past cycles, it is necessary to extract important indicators to reflect the change in battery capacity during the aging process. LSTM algorithm overcomes the gradient instability problem that common CNN may have, and the prediction accuracy in the long-term case is effectively improved [65], hence it should be more suitable for battery capacity estimation under the long-term experiments.

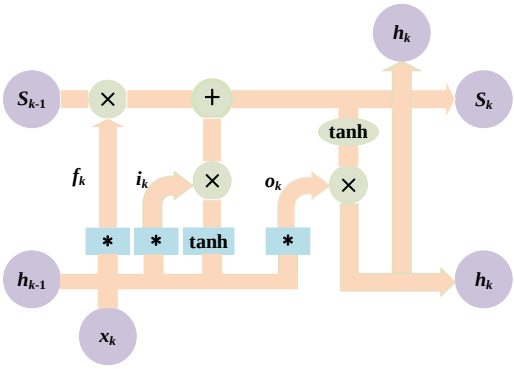


Fig. 1 Overall structure of LSTM

Fig. 1 shows the overall architecture of the LSTM algorithm. The algorithm contains a storage unit with three nonlinear extra gates, including a forgetting gate, input gate, and output gate. In addition, there are four inputs with one output.

$$\begin{cases} f_k = f\left(Q_f . x_k + b_f\right) \\ i_k = f\left(P_i . x_k + b_i\right) \\ \tilde{C}_k = tanh(W_C . x_k + b_C) \\ C_k = \tilde{C}_k * i_k + C_{k-1} * f_k \\ o_k = f(R_o . x_k + b_o) \\ h_k = tanh(C_k) * o_k \end{cases} \quad (2)$$

Eq. (2) lists the calculation formula of each gate and the status update process in the LSTM unit. Wherein, $x_k$ denotes the input data at the current time, $f$ represents the sigmoid function of variable parameters, and $g$ and $h$ are the expressions of hyperbolic activation functions. $R$, $P$, $W$, and $Q$ are weights, $b$ is offset, and $k$ refers to the time step. $f_k$, $i_k$, $\tilde{C}_k$ and $o_k$ are the output of the forget gate, input gate, input node and output gate.

### 2.3 SOH estimation by DACS_LSTM algorithm

The traditional LSTM algorithm has an

obvious problem. In modeling, the uncertainty of hyperparameter selection is very strong, and it is easy to produce overfitting. The number of hidden neurons and the initial learning rate are important hyperparameters. The former is a linear partition of the input features, the higher the number, the higher the model accuracy theoretically. However, the more linearly divided categories, the more distorted the decision boundary, then the appearance of overfitting happened, which reduces the estimation accuracy of the algorithm. The learning rate refers to the rate in the training process of the algorithm. The higher the learning rate is, the faster the training speed is, but the phenomenon of data shock and high loss value is easy occur. The lower the learning rate, the higher the data utilization, but the phenomenon of overfitting is easy to occur, and the low learning rate will also cause the convergence speed of the algorithm to decline. Therefore, for the selection of hyperparameters, a new DACS_LSTM algorithm is designed in this paper to solve this problem effectively.

In this research, the dynamic adaptive cuckoo search algorithm is taken advantage of to optimize the hyperparameters and realize the noise reduction, which effectively improves the modeling accuracy.

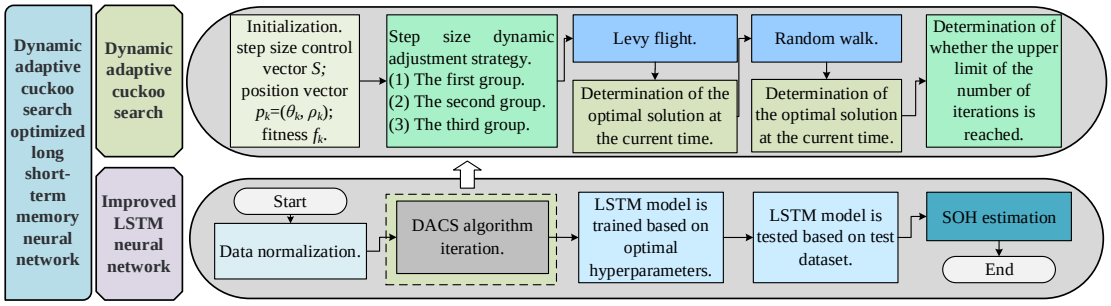


Fig. 2 Flowchart of DACS_LSTM algorithm

Fig. 2 shows the flowchart of the DACS_LSTM algorithm proposed in this paper. It mainly includes data import, data normalization, DACS algorithm iteration, model training, SOH estimation, and estimation error analysis. The specific steps are as follows.

**Step 1** Training dataset and test dataset sample are imported. The amount of training dataset is selected according to the actual situation. In general, the larger the training dataset, the higher the accuracy, however, the problem of running time can not be ignored. At the same time, the test dataset decreases with the increase of the training dataset, which further reduces the reliability of the test and results. In this paper, three scales including 30%, 50%, and 70% of the

dataset are selected as the training dataset.

**Step 2** Data normalization. The purpose of this step is to change the imported data of different orders of magnitude into the same order of magnitude and eliminate the influence of the order of magnitude. The imported data from the training dataset and test dataset are processed respectively, and all data are normalized to the range [0, 1]. The calculation method is shown in Eq. (3).

$$\begin{cases} x_1 = \frac{x_k^{training} - x_{min}^{training}}{x_{max}^{training} - x_{min}^{training}} \\ x_2 = \frac{x_i^{test} - x_{min}^{test}}{x_{max}^{test} - x_{min}^{test}} \end{cases} \quad (3)$$

Wherein, $x_k^{training}$ and $x_1$ represent the original data and normalized data of the training dataset at time $k$, respectively. $x_{min}^{training}$ and $x_{max}^{training}$ represent the minimum and maximum values of the training dataset, respectively. $x_i^{test}$ and $x_2$ represent the original data and normalized data of the test dataset at the time $i$, respectively. $x_{min}^{test}$ and $x_{max}^{test}$ represent the minimum and maximum values of the test dataset, respectively.

**Step 3** DACS algorithm iteration. DACS algorithm optimizes the hyperparameters of the LSTM neural network. In this research, the number of eggs in each nest is 100, and the maximum number of iterations is 500.

Step 3.1 Initialization. $m$ nests are randomly generated, and the position vector $p_k$ of each nest is composed of two components, including the number of hidden neurons $\alpha_k$ and the initial learning rate $\beta_k$ of the LSTM algorithm. The step size control vector $S$ is initialized and the fitness $f_k$ of all $m$ nests is calculated. According to the hyperparameters $\alpha_k$ and $\beta_k$ of the LSTM model contained in the position vector $p_k$ of each nest, the LSTM model is trained according to the training dataset, and the training model $LSTM_k$ is obtained. The training results were compared with reference values. In this paper, the mean square error (MSE) is taken advantage of like the fitness, and the calculation method is shown in Eq. (4).

$$f_k = \frac{1}{D}\sum_{k=1}^{D}\left(O_k - LSTM_k(I_k)\right)^2 \quad (4)$$

Wherein, $D$ is the number of training samples, $I_k$ and $O_k$ refer to the input and output of the training samples respectively. $LSTM_k(I_k)$ refers to the final training results.

Step 3.2 Step size dynamic adjustment strategy. According to the fitness of all nests obtained, the maximum fitness $f_m$, the mean value $f_q$ of all fitness, and the mean value $f_v$ of all fitness exceeding $f_q$ are determined. All the nests are then divided into three categories.

(1) The first group. Nests with more fitness than $f_v$ belong to the first category.

This kind of nest has high fitness and is closest to the global optimal solution, hence the step size control vector is reduced to improve the local search ability. As shown in Eq. (5).

$$S_{k+1} = S_k - \left(S_k - S_{min}\left|\frac{f_q - f_v}{f_m}\right|\right) \quad (5)$$

(2) The second group. Nests with fitness between $f_q$ and $f_v$ are included in the second category. This part of the nest has moderate fitness, hence there is no need to adjust the step size control vector.

(3) The third group. Nests with lower fitness than $f_q$ are included in the third category. This part of the nests have low fitness, and strong local search ability but poor global optimization ability, hence the composition of the step control vector and adaptive control is improved.

$$S_k = 1 - \frac{0.8}{1 + h_1 * e^{-h_2 \Delta}} \quad (6)$$

Wherein, $h_1$, $h_2$, and $\Delta$ are the parameters. When the algorithm stalls, if individuals are distributed and scattered, then $\Delta$ is large. The local optimization capability is enhanced by reducing the component corresponding to the step size in the control vector. The reduction of the component may enhance the global search ability and jump out of the local extremum.

Step 3.3 Levy flight. The new fitness value of the nest is recalculated and compared with the optimal fitness value of the last iteration.

$$\begin{cases} p_{k+1} = p_k + S_k \oplus Levy(\xi) \\ Levy(\xi) \sim u = t^{-\xi}, 1 < \xi \leq 3 \end{cases} \quad (7)$$

Wherein, $\oplus$ represents the entry-wise multiplications, $\xi$ is the Law exponent. The direction of the Levy flight used in this paper obeys a uniform distribution.

Step 3.4 Determination of the optimal solution at the current time. By comparing the fitness of all nests, the one with the highest fitness is found.

Step 3.5 Random walk. According to the initial discovery probability $P_d$, some nests are randomly abandoned, and the abandoned nests are replaced again.

$$p_{k.} = p_k + q_1 \oplus F(q_2 - P_d) \oplus \left(p_{k_1} - p_{k_2}\right) \quad (8)$$

Wherein, $q_1$ and $q_2$ are random numbers that obey uniformly distributed on [0, 1], $p_{k_1}$ and $p_{k_2}$ refer to randomly selected nests, and $F(.)$ represents the step function.

Step 3.6 Determine the optimal solution at the current time. As shown in Eq. (9).

$$p^* = (\alpha^*, \beta^*) \quad (9)$$

Step 3.7 Determination of whether the upper limit of the number of iterations is reached. If so, the loop is ended; otherwise, the operation returns to Step 3.2 to start the iteration again.

**Step 4** LSTM model is trained based on optimal hyperparameters. The position

vector with the highest fitness $p^*$ is selected as the hyperparameter of the LSTM model to construct the optimal LSTM model named $LSTM_{best}$.

**Step 5** LSTM model is tested based on the test dataset. The LSTM optimization model is trained based on the training dataset, and the number of LSTM neurons and the initial learning rate are optimized by the DACS method. The test dataset is taken advantage of to estimate the trained optimal model to normalize the final prediction results.

**Step 6** SOH estimation. The output of the LSTM algorithm is the SOH of the battery, which is calculated through the fully connected layer, as shown in Eq. (10).

$$SOH = f(W_{fo} * h_k + b_{fo}) \quad (10)$$

Wherein, $W_{fo}$ is the expression of the weight matrix between the fully connected layer and the output layer, $b_{fo}$ represents the offset of the layer, and $h_k$ denotes the output of the hidden layer.

## 3. Dataset characteristics analysis and health indicators acquisition

### 3.1 Dataset description and analysis

Two groups of public datasets are selected in this research, dataset A includes CS_35, CS_36, CS_37, CS_38 in CALCE, and dataset B includes B0005, B0006, and B0007 in the NASA dataset. The battery version in CALCE taken advantage of in the experiment is a columnar lithium cobalt oxide battery with a rated capacity of 1.1Ah and a rated voltage of 4.2V. The test battery in NASA dataset is the second generation of 18650-LiCoO2 with a rated capacity of 2Ah and a rated voltage of 4.2V. The four groups of data from dataset A are renamed as $B_1$, $B_2$, $B_3$, and $B_4$, and the three groups of data from dataset B are renamed as $B_5$, $B_6$, and $B_7$ for narrative convenience.

Table 1 Cycle conditions of the datasets A and B

| Datasets | Battery Number | Charging cut-off voltage(V) | Discharging cut-off voltage(V) | Charging constant current(A) | Discharging constant current(A) | Temperature(℃) |
|---|---|---|---|---|---|---|
| A | $B_1$ | 4.2 | 2.7 | 0.55 | 1.1 | 25 |
| | $B_2$ | 4.2 | 2.7 | 0.55 | 1.1 | 25 |
| | $B_3$ | 4.2 | 2.7 | 0.55 | 1.1 | 25 |
| | $B_4$ | 4.2 | 2.7 | 0.55 | 1.1 | 25 |
| B | $B_5$ | 4.2 | 2.7 | 1.5 | 2.0 | 24 |
| | $B_6$ | 4.2 | 2.5 | 1.5 | 2.0 | 24 |
| | $B_7$ | 4.2 | 2.2 | 1.5 | 2.0 | 24 |

Table 1 shows the aging test cycle conditions of seven groups of batteries

belonging to two datasets. For dataset A, a complete charge and discharge test consisted of a constant current and constant voltage (CC-CV) charging process at 0.55 A and a constant current (CC) discharge stage at 1.1 A. The cycle is repeated until the experiment is stopped when the battery capacity decreased by 30%. It can be seen that the experimental conditions are the same, which is conducive to the extraction of health indicators in the next step. For dataset B, the discharge cut-off voltages of the three groups of batteries are different, which are 2.7V, 2.5V, and 2.2V respectively, which may affect the aging process of the batteries.

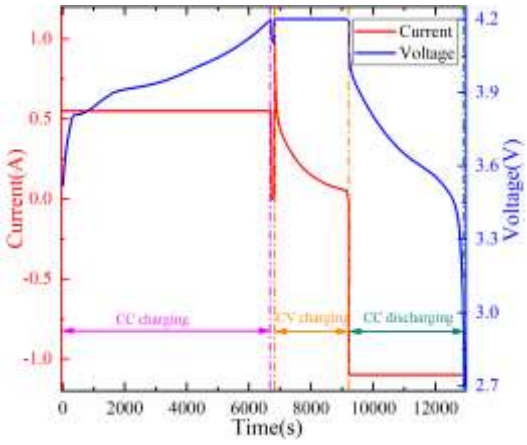


(i) Charging-discharging curves of $B_1$

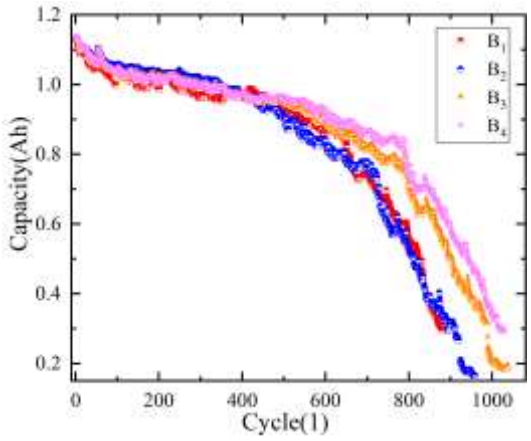


(ii) Capacity degradation curves of $B_1$~$B_4$

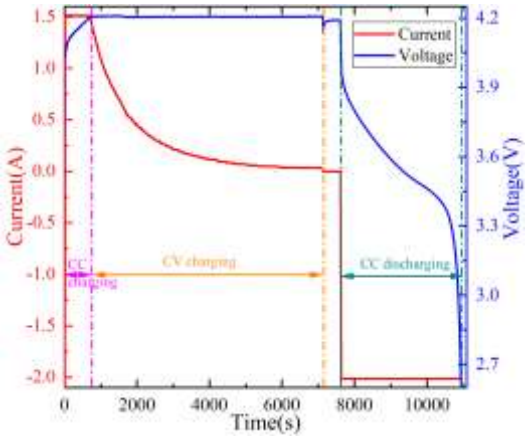


(iii) Charging-discharging curves of $B_5$

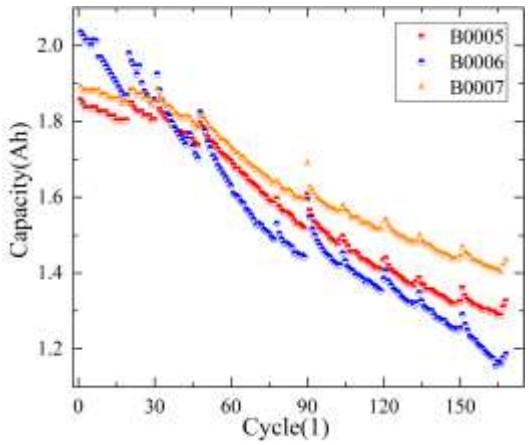


(iv) Capacity degradation curves of $B_5$~$B_7$

Fig. 3 Complete charging-discharging cycle and capacity degradation curves of $B_1$~$B_4$ and $B_5$~$B_7$

Fig. 3 (i) shows the current and voltage change process under a charge-discharge cycle of $B_1$. The battery is first charged at a constant current of 0.55 A (0.5 C) until the voltage rises to 4.2 V. A very short shelving period is followed immediately by constant voltage charging at 4.2 V until the current drops to 0.05 A. The charging stage is constant discharge at 1.1 A (1C) until the voltage drops to 2.7 V. Fig. 3 (ii) shows the

capacity degradation curves of four datasets from $B_1$ to $B_4$ in the whole life cycle. Even under the same experimental conditions and with the same type of battery, the aging processes of capacity are not the same. Compared with $B_1$ and $B_2$, the aging speed of $B_3$ and $B_4$ is significantly slower. This shows that even batteries of the same version can exhibit very different attenuation patterns when tested under the same conditions. Fig. 3 (iii) shows the current and voltage in a complete charge-discharge cycle of $B_5$. After a CC charge at 1.5A, the battery voltage rises to 4.2V, and then a CV charge is carried out until the battery current drops to 0.05A. Next, a CC charge of 2.0A is applied until the voltage drops to 2.7V. Fig. 3 (iv) shows the capacity degradation curves of $B_5$~$B_7$. Similarly, the aging rate of the three batteries is also quite different. Therefore, it is necessary to analyze the SOH estimation results of seven groups of data simultaneously.

### 3.2 Health indicators selection and acquisition

The current, voltage, charging time, and some other variables can effectively reflect the aging of the battery. In this paper, nine variables are selected as HIs by analyzing the changing laws of each parameter during the experiment. Seven are measured factors and two are calculated. Measured HIs could more easily get directly from the dataset, mainly including three categories, respectively are associated with the current, voltage, and charging time.

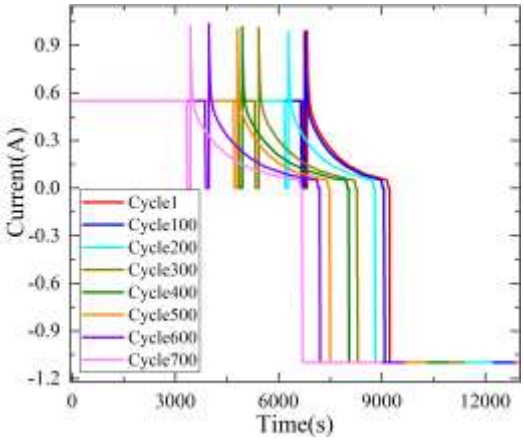


(i) Current curves in different cycles of $B_1$

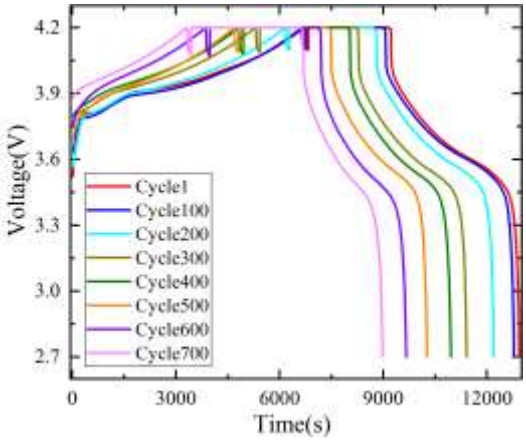


(ii) Voltage curves in different cycles of $B_1$

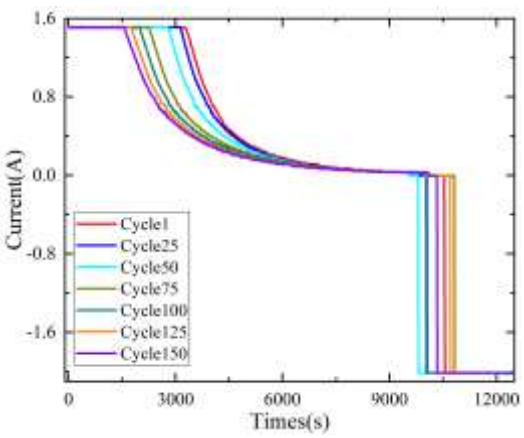


(iii) Current curves in different cycles of $B_5$

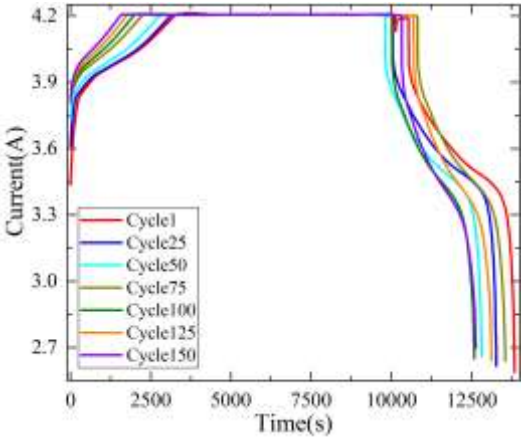


(iv) Voltage curves in different cycles of $B_5$

Fig. 4 Current and voltage curves of $B_1$ and $B_5$

1) Current-related HIs. The current of the battery in the charging phase changed obviously with the continuous charging and discharging cycle. As shown in Fig. 4 (i) and (iii), as the number of cycles increased, the current curve at the charging stage moved to the left, indicating that the duration of the constant current stage gradually decreased. Based on this situation, three types of HIs were selected, including $C_h$, $C_{c,}$ and $C_V$, which were the area of the current curve of the whole charging stage, the constant current charging stage, and the constant voltage stage.

2) Voltage-related HIs. Fig. 4 (ii) and (iv) show that the voltage curve changes. As the battery ages, the capacity decreases, while the charging current did not change, hence the voltage rises faster and showed the same trend as the current. The voltage increase $\triangle U$ at the same time during the charging stage became the option of the related HI.

3) Charging time-related HIs. According to HIs related to current and voltage, the total charging and discharging time of the battery would gradually shorten with the aging process. Here, the duration of constant current phase $t_c$, duration of constant voltage stage $t_v$, and the ratio of the constant current time to total charging time $r_c$ are selected as HIs.

HIs obtained by measurement often cannot further show the deeper battery health change characteristics. Hence, the other HIs are obtained other through calculation. Incremental capacity (IC) curves are obtained by analyzing the variation of battery capacity with voltage over a short period. In this research, the IC curve is further obtained through the voltage curve of the battery, as shown in Eq. (11).

$$\frac{dQ}{dV} = I \cdot \frac{dt}{dV} = \frac{I}{\frac{dV}{dt}} \tag{11}$$

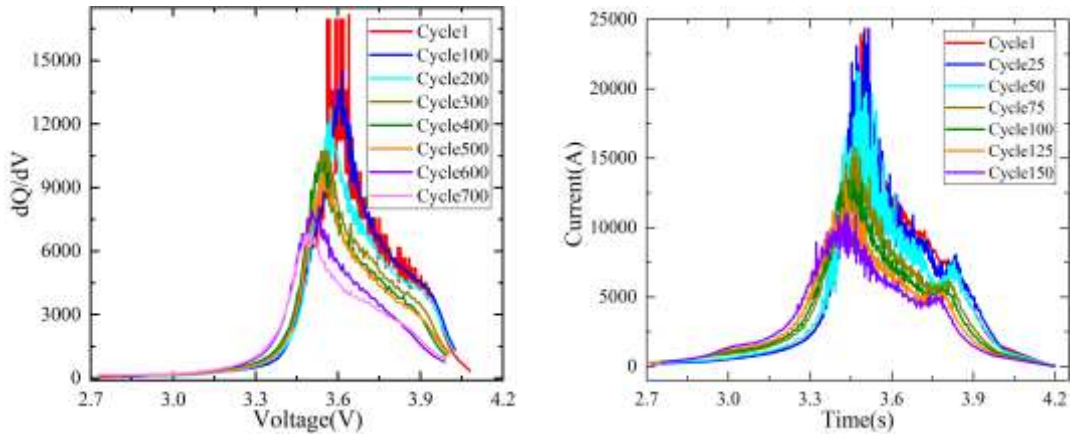


(i) IC curves of $B_1$ (ii) IC curves of $B_5$

Fig. 5 IC curves of different cycles of $B_1$ and $B_5$

Fig. 5 shows the IC curve of the $B_1$ and $B_5$ batteries. Following the cycle continues, IC curve peak $P_{IC}$ gradually decreases, and the peak position $P_{ICP}$ shifts to the left, both of which has obvious and regular changes. Therefore, these two indexes are selected as HIs.

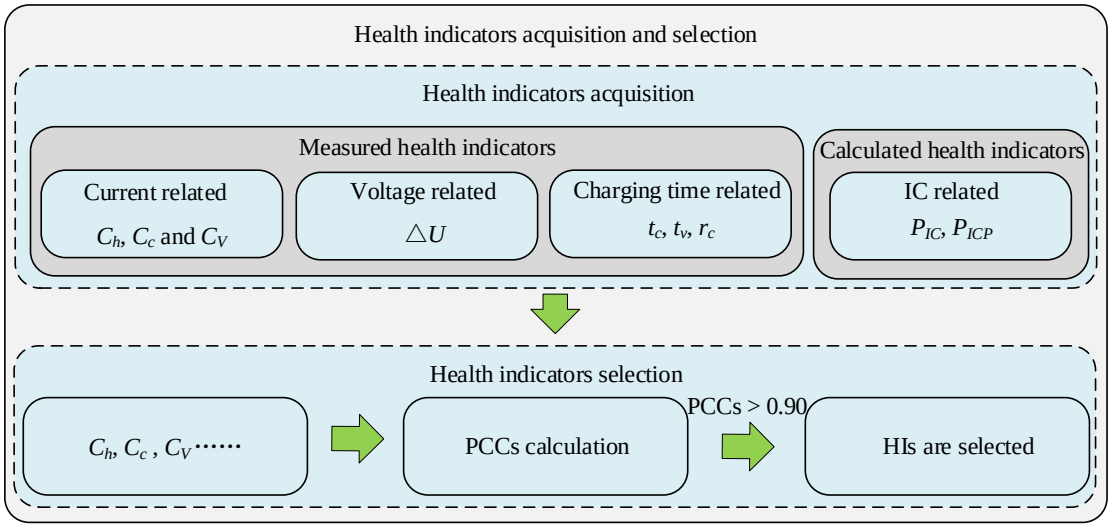


Fig. 6 Health indicators acquisition and selection

Fig. 6 shows the extraction process of HIs used. In summary, a total of nine indicators related to current, voltage, charging time, and IC curve is selected as HIs of the battery. The Pearson correlation coefficient (PCC) is selected to measure the linear correlation between HIs and SOH reference, as shown in Eq. (12).

$$PCCs = \frac{\sum_{i=1}^{n}(z_i-\overline{z})(q_i-\overline{q})}{\sqrt{\sum_{i=1}^{n}(z_i-\overline{z})^2}\sqrt{\sum_{i=1}^{n}(q_i-\overline{q})^2}} \quad (12)$$

Wherein, $z$ represents HIs, and $q$ is the reference value of SOH. The value range of this coefficient is [-1, 1]. When PCCs are 1 or -1, it indicates that there is a complete positive linear correlation or negative linear

correlation between two variables. 0 means there is no linear correlation at all.

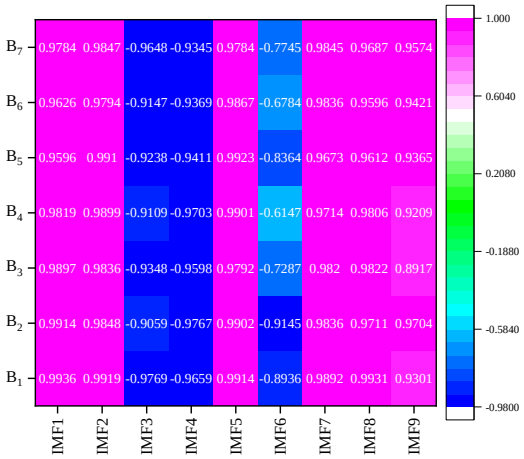


Fig. 7 PCCs results for each group data in datasets A and B

The calculation results of PCCs of seven groups of data are shown in **Error! Reference source not found.**, indicating that most of the related parameters could well reflect the aging mechanism of the battery. HIs with a correlation over 0.9 are selected for model training in this paper.

### 3.3 SOH evaluation framework

On account of the DACS_LSTM algorithm proposed in Section 2.3, the total SOH estimation network is proposed, as shown in Fig. 8. The overall structure of the proposed method includes data processing, offline model training, and online SOH estimation.

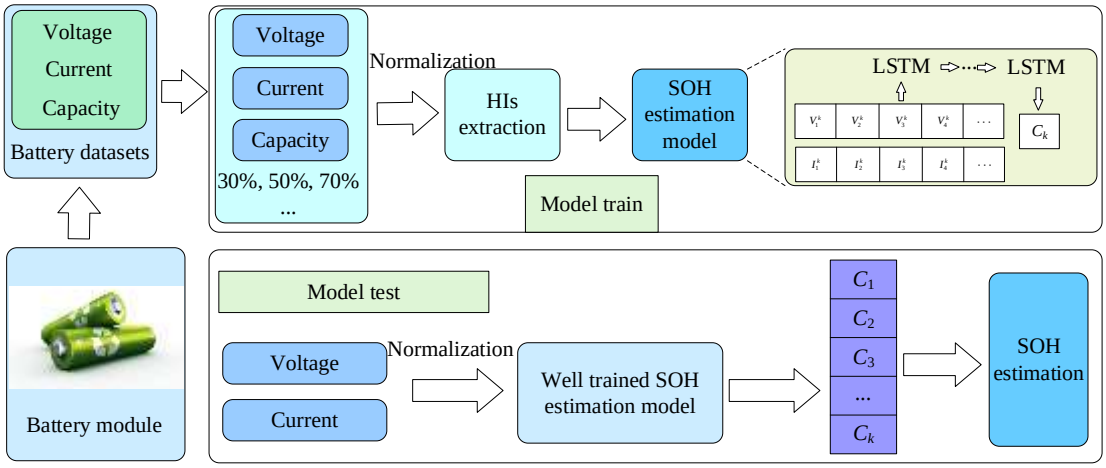


Fig. 8 Framework of SOH estimation

Data processing includes data analysis, HIs extraction, and selection. Firstly, 30%, 50%, or 70% of the total dataset is selected as the training dataset to carry out HIs extraction, and the rest of the data is used as a test dataset. Then, the scale of the current, voltage, and capacity in the training dataset and test dataset is normalized respectively. After the HIs extraction, PCC is used to evaluate the linear correlation between health indicators and state of health. Then, HIs are taken advantage of as the input of the proposed DACS_LSTM algorithm. Through offline model training, the optimal

hyperparameters of the model are obtained by using the training dataset based on the DACS algorithm. Finally, based on the trained model, the SOH estimation of the battery is realized in the online test dataset and the performance of the model proposed is evaluated.

## 4. SOH estimation results

### 4.1 Evaluation indexes for SOH estimation

To evaluate the performance of the proposed algorithm effectively, several kinds of error indexes are selected, including mean absolute error (MAE), root mean square error (RMSE), mean absolute percentage error (MAPE), and R_square (R2). MAE refers to the average of the absolute value of the deviation from the arithmetic mean of all individual observations, which better reflects the prediction error. RMSE represents the square root of the ratio of the square of the deviation between the observed value and the true value and the number of observations n, which is used to measure the deviation between the observed value and the true value. MAPE is taken advantage of to measure the relative percentage error between the estimate and the actual value. R2 is the determination coefficient, which is utilized to judge model quality. The calculation methods of all parameters are shown in Eq. (13).

$$\begin{cases} MAE = \frac{1}{n}\sum_{k=1}^{n}\left|\hat{SOH}_k - SOH_k\right| \\ RMSE = \sqrt{\frac{1}{n}\sum_{k=1}^{n}\left(\hat{SOH}_k - SOH_k\right)^2} \\ MAPE = \frac{1}{n}\sum_{k=1}^{n}\left|\frac{\hat{SOH}_k - SOH_k}{SOH_k}\right| \times 100\% \\ R2 = 1 - \frac{\sum_k\left(\hat{SOH}_k - SOH_k\right)^2}{\sum_k\left(\bar{SOH}_k - SOH_k\right)^2} \end{cases} \tag{13}$$

Wherein, $\hat{SOH}_k$, $SOH_k$ and $\bar{SOH}_k$ refer to the estimates, reference values, and averages of the state of health, respectively. $n$ denotes the number of test samples. The smaller MAE, RMSE, and MAPE are, the higher the estimation accuracy of SOH is, and the larger R2 is, the better the model fitting degree is.

### 4.2 Capacity estimation effect under different hyperparameter Settings

In order to prove the influence of hyperparameter settings on the prediction results of battery degradation trend, $B_5$ of NASA dataset and $B_1$ data of CALCE dataset are taken as the training set, the data accounting for 50% of the total is taken as the training dataset, and the different number of hidden neurons and the initial learning rate is selected based on LSTM algorithm to carry out SOH estimation. The results are shown in Fig. 9.

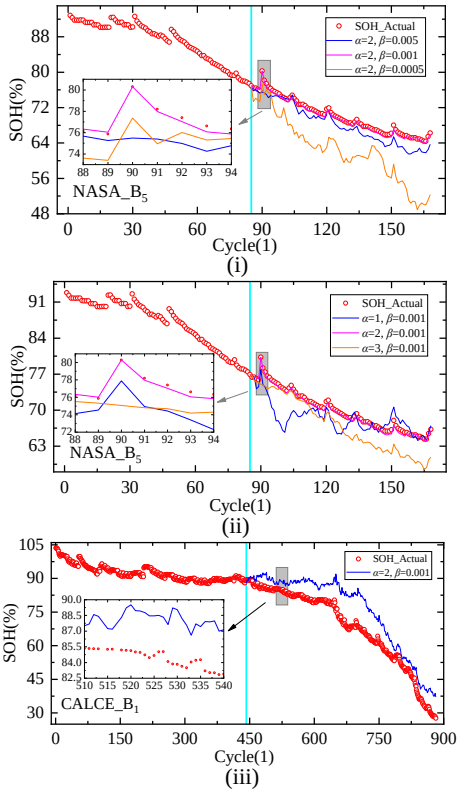


Fig. 9 SOH estimation results $B_5$ and $B_1$ based on LSTM algorithm with different numbers of hidden nerves and initial learning rate

In Fig. 9 (i), with the increase in the initial learning rate, the prediction results have a significant change. When the number of hidden neurons and the initial learning rate are 2 and 0.005, respectively, the estimation results at the beginning are more consistent with the changing trend of the training dataset, while the deviation from the test dataset is large, indicating the occurrence of overfitting. However, when the number of hidden nerves and the initial learning rate are 2 and 0.001 respectively, the estimation results are relatively good, and the attenuation trend of the test dataset can be roughly predicted. When the number of hidden neurons and the initial learning rate are 0 and 0.0005 respectively, the degradation tendency of the training dataset or test dataset cannot be fitted effectively and show serious divergence, attribute to the initial learning rate being too large, which causes serious losses and data shocks.

In Fig. 9 (iii), when the number of hidden nerves selected and the initial learning rate are both 2 and 0.001, the estimation effect is much worse, which indicates that there are also great differences in the selection of hyperparameters under different battery types. Therefore, the selection of these two hyperparameters based on experience alone is unreliable and inefficient.

### 4.3 Health evaluation results under multiple training-scales

In this paper, three different training scales of 30%, 50%, and 70% were selected. Four groups of aging datasets including $B_1$, $B_2$, $B_3$, and $B_4$ are chosen to verify the performance of the algorithm, and the most common LSTM and convolutional neural network long short-term memory (CNN_LSTM) algorithms established by Toughzaoui et al. [66], is taken advantage of as the reference, and the results of the SOH are obtained.

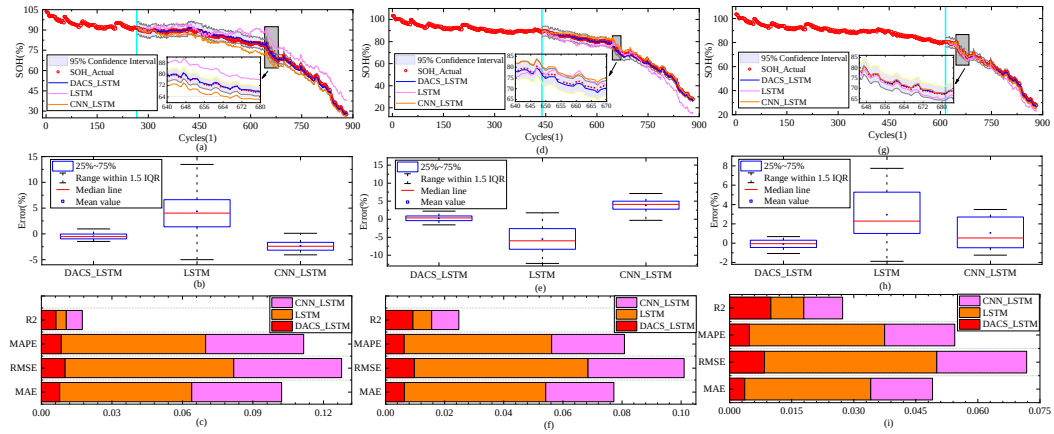


(i) Results for $B_1$

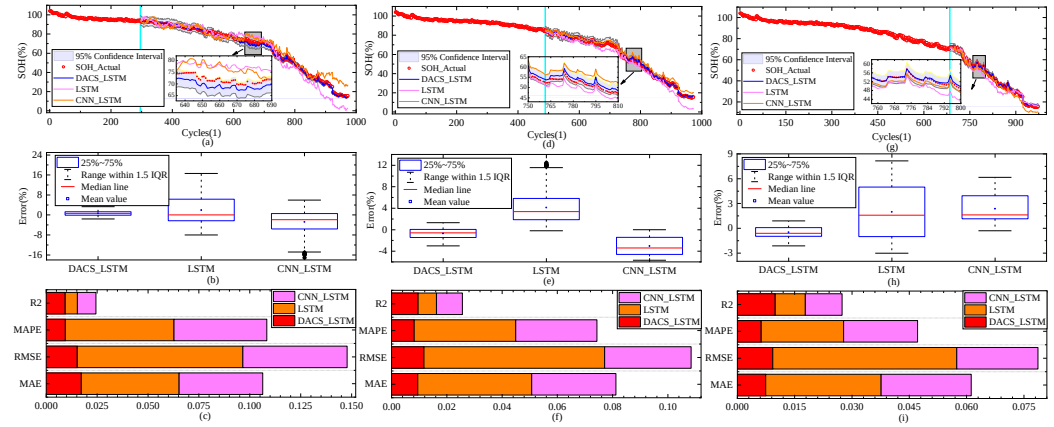


(ii) Results for $B_2$

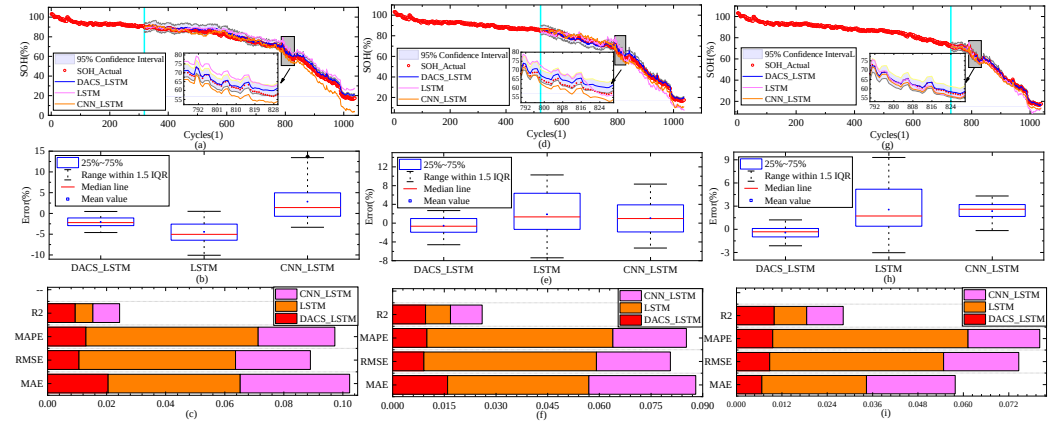


(iii) Results for $B_3$

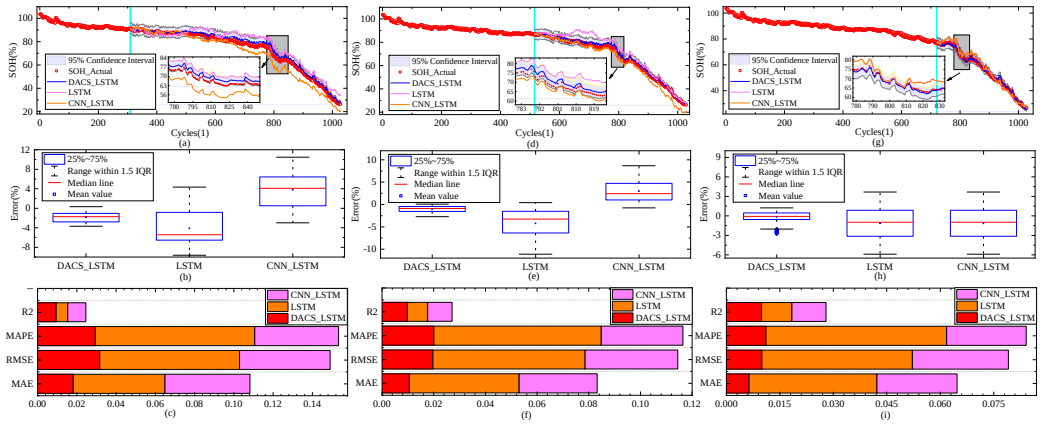


(iv) Results for $B_4$

Fig. 10 SOH estimation results of $B_1$~$B_4$ under multiple training-scales

Fig. 10 SOH estimation results of $B_1$~$B_4$ (i)~(iv) shows the SOH estimation results, error range, and performance evaluation results of three methods under four datasets in three training scales. It can be seen that after the addition of the optimization algorithm, the accuracy and convergence of the algorithm are improved obviously after the optimization of the hyperparameters $\alpha$ and $\beta$. Under the three training scales, compared with the comparison algorithm, the proposed DACS_LSTM algorithm shows the highest accuracy, the estimation results are closest to the actual SOH and the true value of the SOH is all included within the 95% confidence interval of the estimated result of the algorithm in each cycle. For $B_1$, when the training scale is 70%, the estimation error of the method proposed in this paper can be controlled by 2% in each cycle. In the same case, the maximum error of LSTM is over 7%, while that of CNN_LSTM is close to 4%. At the same time, the performance evaluation results indicate that the estimated model established by DACS_LSTM also has obvious advantages in the stability of estimation results over the comparison algorithm, and showing the best performance. The SOH estimation results of the other three datasets also show that the estimation results of the proposed algorithm are highly consistent with the reference values. In addition, the SOH estimation for B0005~B0007 datasets is shown in Fig. 11.

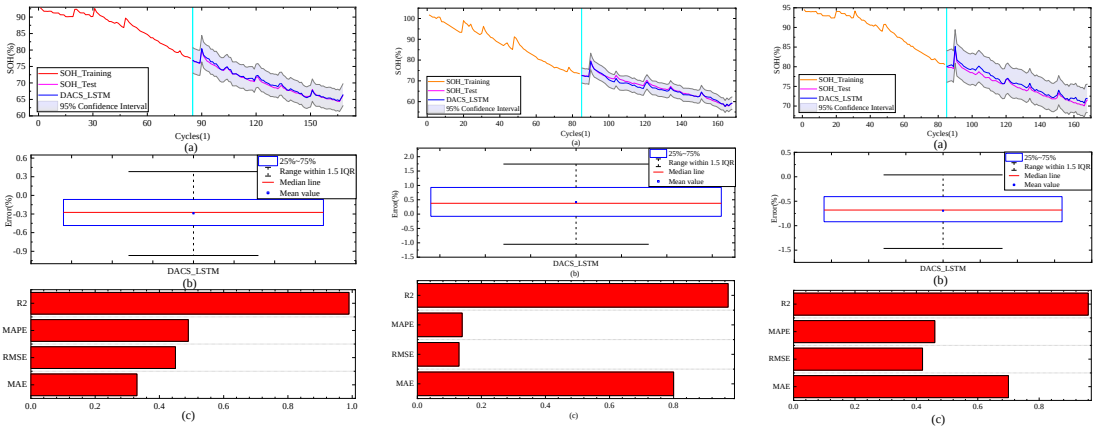


(i) Results for $B_5$ (ii) Results for $B_6$ (iii) Results for $B_7$

Fig. 11 SOH estimation results of $B_5$~$B_7$ under 50% training-scales

In Fig. 11, the DACS_LSTM algorithm proposed in this paper still maintains high accuracy when predicting the aging trend of different types of batteries and different operating conditions. The error can be kept within 2%, MAPE and RMSE within 0.5%, MAE within 1%, and R2 above 0.95. The result indicates that the algorithm has generalization applications for different batteries.

### 4.4 Accuracy and robustness analysis of the algorithm

According to the indexes for SOH estimation accuracy given in Section 4.1, the estimation performance of the DACS_LSTM algorithm under different training scales and different battery datasets is quantitatively evaluated, and the results are obtained.

Table 2 Comparison of estimation results between DACS_LSTM and other methods

| Batteries | Training scales | Methods | MAE (%) | RMSE (%) | MAPE (%) | R2 |
|---|---|---|---|---|---|---|
| $B_1$ | 30% | DACS_LSTM | 0.78 | 1.01 | 0.85 | 0.95 |
| | | LSTM | 5.62 | 7.17 | 6.14 | 0.44 |
| | | CNN_LSTM | 3.82 | 4.59 | 4.17 | 0.68 |
| | 50% | DACS_LSTM | 0.64 | 0.98 | 0.63 | 0.98 |
| | | LSTM | 4.78 | 5.88 | 4.99 | 0.63 |
| | | CNN_LSTM | 2.30 | 3.25 | 2.47 | 0.92 |
| | 70% | DACS_LSTM | 0.37 | 0.84 | 0.48 | 1.00 |
| | | LSTM | 3.04 | 4.16 | 3.27 | 0.79 |
| | | CNN_LSTM | 1.50 | 2.17 | 1.69 | 0.94 |
| $B_2$ | 30% | DACS_LSTM | 1.72 | 1.52 | 0.94 | 0.96 |
| | | LSTM | 4.81 | 8.14 | 5.34 | 0.60 |
| | | CNN_LSTM | 4.11 | 5.11 | 4.56 | 0.91 |
| | 50% | DACS_LSTM | 0.95 | 1.17 | 0.82 | 0.97 |
| | | LSTM | 4.12 | 6.54 | 3.67 | 0.66 |

| | | | | | | |
|---|---|---|---|---|---|---|
| | | CNN_LSTM | 3.05 | 3.13 | 2.94 | 0.94 |
| | | DACS_LSTM | 0.74 | 0.93 | 0.62 | 0.99 |
| | 70% | LSTM | 3.02 | 4.81 | 2.16 | 0.79 |
| | | CNN_LSTM | 2.36 | 2.13 | 1.94 | 0.96 |
| | | DACS_LSTM | 2.05 | 1.06 | 1.30 | 0.95 |
| | 30% | LSTM | 4.47 | 5.30 | 5.83 | 0.60 |
| | | CNN_LSTM | 3.71 | 2.54 | 2.60 | 0.91 |
| | | DACS_LSTM | 1.59 | 0.91 | 1.00 | 0.96 |
| $B_3$ | 50% | LSTM | 4.10 | 5.01 | 5.40 | 0.72 |
| | | CNN_LSTM | 3.10 | 2.15 | 2.13 | 0.92 |
| | | DACS_LSTM | 0.67 | 0.88 | 0.96 | 1.00 |
| | 70% | LSTM | 2.77 | 4.60 | 5.17 | 0.86 |
| | | CNN_LSTM | 2.35 | 1.99 | 1.90 | 0.97 |
| | | DACS_LSTM | 1.82 | 2.97 | 2.95 | 0.95 |
| | 30% | LSTM | 4.67 | 7.12 | 8.12 | 0.59 |
| | | CNN_LSTM | 4.33 | 4.62 | 4.27 | 0.92 |
| | | DACS_LSTM | 1.06 | 1.97 | 2.01 | 0.98 |
| $B_4$ | 50% | LSTM | 4.25 | 5.89 | 6.48 | 0.78 |
| | | CNN_LSTM | 3.02 | 3.59 | 3.16 | 0.95 |
| | | DACS_LSTM | 0.63 | 1.00 | 1.11 | 0.99 |
| | 70% | LSTM | 3.59 | 4.22 | 5.07 | 0.85 |
| | | CNN_LSTM | 2.25 | 2.70 | 2.23 | 0.96 |

Table 2 shows the estimation errors and fitting performance results of the three algorithms in the four groups of data including $B_1$~$B_4$ under three training scales. The MAE of the algorithms proposed in this paper is basically below 2%, and R2 exceeds 0.95. As can be seen from Section 3.1, the decay rates of $B_1$, $B_2$, and $B_3$, $B_4$ are quite different. Therefore, the results show that the algorithm maintains an excellent SOH estimation effect for different decay conditions. In contrast, the estimation accuracy of LSTM and CNN_LSTM varies greatly under different datasets, and the application breadth is not wide. No matter RMSE or MAPE, the DACS_LSTM algorithm has obvious improvement compared with the other two algorithms. Experimental results show that the DACS_LSTM method has good validity, accuracy, and convergence in the SOH estimation of lithium-ion batteries.

Based on the $B_5$~$B_7$ from the NASA dataset, the latest several algorithms including random forest convolutional neural network (RF-CNN) proposed by Yang et al. [67], backpropagation long short-term memory (B_LSTM) proposes by

Gong et al. [65], particle swarm optimization long short-term memory (PSO_LSTM) algorithm and differential evolution grey wolf optimizer long short-term memory (DEGWO-LSTM) presents by Ma et al. [61], and simplified pseudo-two-dimensional (S_P2D) raises by Liu et al. [68], are utilized as the comparison, as shown in Table 3.

Table 3 Comparison of estimation results between DACS_LSTM and other latest reference

| Methods | MAE (%) | RMSE (%) | MAPE (%) | R2 |
|---|---|---|---|---|
| DACS_LSTM | 0.82 | 0.45 | 0.49 | 0.96 |
| GA-PSO-SVR | - | 3.52 | 3.72 | - |
| RF-CNN | 1.51 | - | - | - |
| S_P2D | 1.62 | - | - | - |
| PSO_LSTM | 3.35 | 3.95 | 4.95 | 0.83 |
| DEGWO-LSTM | 2.08 | 2.43 | 3.02 | 0.93 |
| B_LSTM | - | 2.6 | - | - |

In Table 3, MAE, RMSE, and MAPE are the maximum values in the SOH estimation in each method, and R2 is the minimum value. Compared with the two optimization algorithm including PSO and DEGWO, the MAE of LSTM based on the DACS algorithm is 75.52% and 60.58% lower, RMSE is 88.61% and 81.48% lower, MAPE is 90.10% and 83.77% lower, and R2 is 15.67% and 3.23% higher, respectively. Meanwhile, compared with the latest proposed machine learning methods such as GA-PSO-SVR, RF-CNN, S_P2D, and B_LSTM, the algorithm proposed by the research also shows the best performance. From the experimental tests, it can be observed that the DACS_LSTM-based SOH estimation result has the optimal accuracy with the least uncertainty, which verifies its accuracy and robustness.

## 5. Conclusions and future work

In this paper, the state of health assessment issues of lithium-ion batteries based on the improved long short-term memory neural network model with multi-training scales and multi-dimensional health indicators is studied. After the high degree of correlation with the state of health is verified, nine health indicators are obtained through measurement and calculation, therefore, a large number of factors can exert influence on the state of health of batteries that are mined effectively. Meanwhile, a dynamic adaptive cuckoo search long short-term memory neural network algorithm is proposed by combining the improved cuckoo search strategy with the long short-term memory

neural network to realize an accurate estimation of the state of health of four aging datasets under three training scales. The results show that the maximum mean absolute error of the proposed algorithm compared with the comparison algorithm including long short-term memory neural network and convolutional neural network long short-term memory algorithms decrease by 63.5% and 52.7%, respectively, the maximum root mean square error is reduced by 63.5% and 41.9%, respectively, the maximum mean absolute percentage error decreases by 63.7% and 35.3%, respectively, and the minimum R_square increases by 115.9% and 39.7%, respectively. At the same time, compared with other optimization algorithms and the latest machine learning algorithms, the proposed method also shows the highest accuracy and strongest convergence. The results indicate the performance of the proposed algorithm has a significant advantage.

In summary, this research establishes a class of effective lithium-ion battery state of health evaluation methods based on the combination of filtering algorithm and neural network methods, which provides effective assessment and health management strategy for a battery management system with high accuracy. To further improve this research, the next work mainly includes the following. Firstly, the estimation method of the state of health can be further enriched, and the state of health estimation from the perspectives of battery capacity and internal resistance can be comprehensively considered. Secondly, the different operating environments of the battery can be subdivided, and the health management under various conditions such as temperature and humidity, and high and low pressure can be considered. Finally, the complexity of the algorithm can be reduced to further improve practicability.

**Acknowledgments**

The work is supported by the National Natural Science Foundation of China (No. 62173281, 61801407), Sichuan science and technology program (No. 2019YFG0427), China Scholarship Council (No. 201908515099), and Fund of Robot Technology Used for Special Environment Key Laboratory of Sichuan Province (No. 18kftk03).

## CRediT author statement

**Pu Ren**: Conceptualization, Methodology, Software, and Writing.

**Shunli Wang**: Visualization, Investigation.

**Xianpei Chen**: Supervision.

**Heng Zhou**: Software, Validation.

**Carlos Fernandez**: Data curation, Original draft preparation.

**Daniel-Ioan Stroe**: Writing- Reviewing and Editing.

**Declaration of interests**

The authors declare that they have no known competing financial interests or personal relationships that could have appeared to influence the work reported in this paper.

**Reference**


1. H.T. Shi, L.P. Wang, S.L. Wang, C. Fernandez, X. Xiong, B.E. Dablu, W.H. Xu, A novel lumped thermal characteristic modeling strategy for the online adaptive temperature and parameter co-estimation of vehicle lithium-ion batteries, Journal Of Energy Storage, 50 (2022) 169-185 DOI: 10.1016/j.est.2022.104309.
2. J. Zhu, Y. Wang, Y. Huang, R.B. Gopaluni, Y. Cao, M. Heere, M.J. Muhlbauer, L. Mereacre, H. Dai, X. Liu, A. Senyshyn, X. Wei, M. Knapp, H. Ehrenberg, Data-driven capacity estimation of commercial lithium-ion batteries from voltage relaxation, Nature Communications, 13 (2022) 136~157 DOI: 10.1038/s41467-022-29837-w.
3. J. Zhu, M.S.D. Darma, M. Knapp, D.R. Sorensen, M. Heere, Q. Fang, X. Wang, H. Dai, L. Mereacre, A. Senyshyn, X. Wei, H. Ehrenberg, Investigation of lithium-ion battery degradation mechanisms by combining differential voltage analysis and alternating current impedance, Journal of Power Sources, 448 (2020) 324~339 DOI: 10.1016/j.jpowsour.2019.227575.
4. H.T. Shi, S.L. Wang, C. Fernandez, C.M. Yu, W.H. Xu, B.E. Dablu, L.P. Wang, Improved multi-time scale lumped thermoelectric coupling modeling and parameter dispersion evaluation of lithium-ion batteries, Applied Energy, 324 (2022) 1123-1149 DOI: 10.1016/j.apenergy.2022.119789.
5. H.T. Shi, S.L. Wang, L.P. Wang, W.H. Xu, C. Fernandez, B.E. Dablu, Y.C. Zhang, On-line adaptive asynchronous parameter identification of lumped electrical

characteristic model for vehicle lithium-ion battery considering multi-time scale effects, Journal of Power Sources, 517 (2022) 248-269 DOI: 10.1016/j.jpowsour.2021.230725.

6. B.O. Agudelo, W. Zamboni, E. Monmasson, Application domain extension of incremental capacity-based battery SoH indicators, Energy, 234 (2021) 2189-2206 DOI: 10.1016/j.energy.2021.121224.
7. X.L. Bian, Z.B. Wei, J.T. He, F.J. Yan, L.C. Liu, A Novel Model-Based Voltage Construction Method for Robust State-of-Health Estimation of Lithium-Ion Batteries, Ieee Transactions on Industrial Electronics, 68 (2021) 12173-12184 DOI: 10.1109/Tie.2020.3044779.
8. X.L. Bian, Z.G. Wei, W.H. Li, J. Pou, D.U. Sauer, L.C. Liu, State-of-Health Estimation of Lithium-Ion Batteries by Fusing an Open Circuit Voltage Model and Incremental Capacity Analysis, Ieee Transactions on Power Electronics, 37 (2022) 2226-2236 DOI: 10.1109/Tpel.2021.3104723.
9. Z. Chen, H.Q. Zhao, Y.J. Zhang, S.Q. Shen, J.W. Shen, Y.G. Liu, State of health estimation for lithium-ion batteries based on temperature prediction and gated recurrent unit neural network, Journal of Power Sources, 521 (2022) 1453-1469 DOI: 10.1016/j.jpowsour.2021.230892.
10. L. Feng, L.H. Jiang, J.L. Liu, Z.Y. Wang, Z.S. Wei, Q.S. Wang, Dynamic overcharge investigations of lithium ion batteries with different state of health, Journal of Power Sources, 507 (2021) 4897-4916 DOI: 10.1016/j.jpowsour.2021.230262.
11. C.H. Zhang, Y.Z. Kang, B. Duan, Z.K. Zhou, Q. Zhang, Y.L. Shang, A.L. Chen, An Adaptive Battery Capacity Estimation Method Suitable for Random Charging Voltage Range in Electric Vehicles, Ieee Transactions on Industrial Electronics, 69 (2022) 9121-9132 DOI: 10.1109/Tie.2021.3111585.
12. Z.W. Deng, X.K. Lin, J.W. Cai, X.S. Hu, Battery health estimation with degradation pattern recognition and transfer learning, Journal of Power Sources, 525 (2022) 2541-2562 DOI:

10.1016/j.jpowsour.2022.231027.

13. A. Chu, A. Allam, A.C. Arenas, G. Rizzoni, S. Onori, Stochastic capacity loss and remaining useful life models for lithium-ion batteries in plug-in hybrid electric vehicles, Journal of Power Sources, 478 (2020) 324-339 DOI: 10.1016/j.jpowsour.2020.228991.
14. Y.M. Fu, J. Xu, M.J. Shi, X.S. Mei, A Fast Impedance Calculation-Based Battery State-of-Health Estimation Method, Ieee Transactions on Industrial Electronics, 69 (2022) 7019-7028 DOI: 10.1109/Tie.2021.3097668.
15. Y.Z. Gao, K.L. Liu, C. Zhu, X. Zhang, D. Zhang, Co-Estimation of State-of-Charge and State-of-Health for Lithium-Ion Batteries Using an Enhanced Electrochemical Model, Ieee Transactions on Industrial Electronics, 69 (2022) 2684-2696 DOI: 10.1109/Tie.2021.3066946.
16. M.F. Ge, Y.B. Liu, X.X. Jiang, J. Liu, A review on state of health estimations and remaining useful life prognostics of lithium-ion batteries, Measurement, 174 (2021) 748-769 DOI: 10.1016/j.measurement.2021.109057.
17. B. Gou, Y. Xu, X. Feng, State-of-Health Estimation and Remaining-Useful-Life Prediction for Lithium-Ion Battery Using a Hybrid Data-Driven Method, IEEE Transactions on Vehicular Technology, 69 (2020) 10854-10867 DOI: 10.1109/Tvt.2020.3014932.
18. X.J. Han, Z.R. Wang, Z.X. Wei, A novel approach for health management online-monitoring of lithium-ion batteries based on model-data fusion, Applied Energy, 302 (2021) 1368-1384 DOI: 10.1016/j.apenergy.2021.117511.
19. Y. Ma, C. Shan, J.W. Gao, H. Chen, A novel method for state of health estimation of lithium-ion batteries based on improved LSTM and health indicators extraction, Energy, 251 (2022) 7164-7181 DOI: 10.1016/j.energy.2022.123973.
20. J.H. Meng, L. Cai, D.I. Stroe, X.R. Huang, J.C. Peng, T.Q. Liu, R. Teodorescu, An Automatic Weak Learner Formulation for Lithium-Ion Battery State of Health Estimation, Ieee Transactions on

Industrial Electronics, 69 (2022) 2659-2668 DOI: 10.1109/Tie.2021.3065594.

21. X. Shu, G. Li, J.W. Shen, Z.Z. Lei, Z. Chen, Y.G. Liu, An adaptive multi-state estimation algorithm for lithium-ion batteries incorporating temperature compensation, Energy, 207 (2020) 178-198 DOI: 10.1016/j.energy.2020.118262.
22. Z.Y. Song, J. Hou, X.F. Li, X.G. Wu, X.S. Hu, H. Hofmann, J. Sun, The sequential algorithm for combined state of charge and state of health estimation of lithium-ion battery based on active current injection, Energy, 193 (2020) 66-77 DOI: 10.1016/j.energy.2019.116732.
23. H.Y. Huang, J.H. Meng, Y.H. Wang, F. Feng, L. Cai, J.C. Peng, T.Q. Liu, A comprehensively optimized lithium-ion battery state-of-health estimator based on Local Coulomb Counting Curve, Applied Energy, 322 (2022) 1522-1539 DOI: 10.1016/j.apenergy.2022.119469.
24. T.C. Ouyang, P.H. Xu, J. Lu, X.Y. Hu, B.L. Liu, N. Chen, Coestimation of State-of-Charge and State-of-Health for Power Batteries Based on Multithread Dynamic Optimization Method, Ieee Transactions on Industrial Electronics, 69 (2022) 1157-1166 DOI: 10.1109/Tie.2021.3062266.
25. B. Jiang, J.G. Zhu, X.Y. Wang, X.Z. Wei, W.L. Shang, H.F. Dai, A comparative study of different features extracted from electrochemical impedance spectroscopy in state of health estimation for lithium-ion batteries, Applied Energy, 322 (2022) 1256-1278 DOI: 10.1016/j.apenergy.2022.119502.
26. B. Tarhan, O. Yetik, T.H. Karakoc, Hybrid battery management system design for electric aircraft, Energy, 234 (2021) 353-366 DOI: 10.1016/j.energy.2021.121227.
27. S.L. Wang, S.Y. Jin, D.K. Bai, Y.C. Fan, H.T. Shi, C. Fernandez, A critical review of improved deep learning methods for the remaining useful life prediction of lithium-ion batteries, Energy Reports, 7 (2021) 5562-5574 DOI: 10.1016/j.egyr.2021.08.182.
28. Z.B. Wei, H.K. Ruan, Y. Li, J.W. Li, C.Z. Zhang, H.W. He, Multistage State of Health Estimation of Lithium-Ion Battery With High

Tolerance to Heavily Partial Charging, Ieee Transactions on Power Electronics, 37 (2022) 7432-7442 DOI: 10.1109/Tpel.2022.3144504.

29. Z.C. Xu, J. Wang, P.D. Lund, Y.M. Zhang, Co-estimating the state of charge and health of lithium batteries through combining a minimalist electrochemical model and an equivalent circuit model, Energy, 240 (2022) 3633-3652 DOI: 10.1016/j.energy.2021.122815.
30. F. Liu, C. Shao, W.X. Su, Y. Liu, Online joint estimator of key states for battery based on a new equivalent circuit model, Journal Of Energy Storage, 52 (2022) 264-281 DOI: 10.1016/j.est.2022.104780.
31. R. Sakile, U.K. Sinha, Estimation of State of Charge and State of Health of Lithium-Ion Batteries Based on a New Adaptive Nonlinear Observer, Advanced Theory And Simulations, 4 (2021) 6284-6299 DOI: 10.1002/adts.202100258.
32. J. Wu, X.C. Cui, H. Zhang, M.Q. Lin, Health Prognosis With Optimized Feature Selection for Lithium-Ion Battery in Electric Vehicle Applications, Ieee Transactions on Power Electronics, 36 (2021) 12646-12655 DOI: 10.1109/Tpel.2021.3075558.
33. D.X. Xiao, G.L. Fang, S. Liu, S.Y. Yuan, R. Ahmed, S. Habibi, A. Emadi, Reduced-Coupling Coestimation of SOC and SOH for Lithium-Ion Batteries Based on Convex Optimization, Ieee Transactions on Power Electronics, 35 (2020) 12332-12346 DOI: 10.1109/Tpel.2020.2984248.
34. R. Xiong, Y. Pan, W.X. Shen, H.L. Li, F.C. Sun, Lithium-ion battery aging mechanisms and diagnosis method for automotive applications: Recent advances and perspectives, Renewable & Sustainable Energy Reviews, 131 (2020) 789-803 DOI: 10.1016/j.rser.2020.110048.
35. J. Xu, X.S. Mei, X. Wang, Y.M. Fu, Y.F. Zhao, J.P. Wang, A Relative State of Health Estimation Method Based on Wavelet Analysis for Lithium-Ion Battery Cells, Ieee Transactions on Industrial Electronics, 68 (2021) 6973-6981 DOI: 10.1109/Tie.2020.3001836.
36. Z.C. Xu, J. Wang, P.D. Lund, Y.M. Zhang, Co-estimating the state of charge and health of lithium

batteries through combining a minimalist electrochemical model and an equivalent circuit model, Energy, 240 (2022) 984-1005 DOI: 10.1016/j.energy.2021.122815.

37. S.J. Yang, C.P. Zhang, J.C. Jiang, W.G. Zhang, L.J. Zhang, Y.B. Wang, Review on state-of-health of lithium-ion batteries: Characterizations, estimations and applications, Journal of Cleaner Production, 314 (2021) 412-429 DOI: 10.1016/j.jclepro.2021.128015.

38. Z. Ye, J.B. Yu, State-of-Health Estimation for Lithium-Ion Batteries Using Domain Adversarial Transfer Learning, Ieee Transactions on Power Electronics, 37 (2022) 3528-3543 DOI: 10.1109/Tpel.2021.3117788.

39. M.Q. Lin, C.H. Yan, J.H. Meng, W. Wang, J. Wu, Lithium-ion batteries health prognosis via differential thermal capacity with simulated annealing and support vector regression, Energy, 250 (2022) 3648-3663 DOI: 10.1016/j.energy.2022.123829.

40. J. Wu, L.C. Fang, J.H. Meng, M.Q. Lin, G.Z. Dong, Optimized Multi-Source Fusion Based State of Health Estimation for Lithium-Ion Battery in Fast Charge Applications, Ieee Transactions on Energy Conversion, 37 (2022) 1489-1498 DOI: 10.1109/Tec.2021.3137423.

41. Z.Q. Lyu, G. Wang, R.J. Gao, Synchronous state of health estimation and remaining useful lifetime prediction of Li-Ion battery through optimized relevance vector machine framework, Energy, 251 (2022) 361-378 DOI: 10.1016/j.energy.2022.123852.

42. X.F. Sun, K. Zhong, M. Han, A hybrid prognostic strategy with unscented particle filter and optimized multiple kernel relevance vector machine for lithium-ion battery, Measurement, 170 (2021) 1354-1369 DOI: 10.1016/j.measurement.2020.108679.

43. Z.W. Deng, X.S. Hu, P.H. Li, X.K. Lin, X.L. Bian, Data-Driven Battery State of Health Estimation Based on Random Partial Charging Data, Ieee Transactions on Power Electronics, 37 (2022) 5021-5031 DOI: 10.1109/Tpel.2021.3134701.

44. X.Y. Li, C.G. Yuan, Z.P. Wang, J.L.

Xie, A data-fusion framework for lithium battery health condition Estimation Based on differential thermal voltammetry, Energy, 239 (2022) 3267-3285 DOI: 10.1016/j.energy.2021.122206.

45. G.Z. Dong, W.J. Han, Y.J. Wang, Dynamic Bayesian Network-Based Lithium-Ion Battery Health Prognosis for Electric Vehicles, Ieee Transactions on Industrial Electronics, 68 (2021) 10949-10958 DOI: 10.1109/Tie.2020.3034855.

46. M. Haris, M.N. Hasan, S.Y. Qin, Early and robust remaining useful life prediction of supercapacitors using BOHB optimized Deep Belief Network, Applied Energy, 286 (2021) 3578-3599 DOI: 10.1016/j.apenergy.2021.116541.

47. K.S.R. Mawonou, A. Eddahech, D. Dumur, D. Beauvois, E. Godoy, State-of-health estimators coupled to a random forest approach for lithium-ion battery aging factor ranking, Journal of Power Sources, 484 (2021) 3697-3711 DOI: 10.1016/j.jpowsour.2020.229154.

48. Z.Y. Xu, Y.J. Guo, J.H. Saleh, A physics-informed dynamic deep autoencoder for accurate state-of-health prediction of lithium-ion battery, Neural Computing & Applications, 34 (2022) 15997-16017 DOI: 10.1007/s00521-022-07291-5.

49. H. Zhang, G.X. Niu, B. Zhang, Q. Miao, Cost-Effective Lebesgue Sampling Long Short-Term Memory Networks for Lithium-Ion Batteries Diagnosis and Prognosis, Ieee Transactions on Industrial Electronics, 69 (2022) 1958-1967 DOI: 10.1109/Tie.2021.3060675.

50. Y. Zhang, Y.F. Li, Prognostics and health management of Lithium-ion battery using deep learning methods: A review, Renewable & Sustainable Energy Reviews, 161 (2022) 369-389 DOI: 10.1016/j.rser.2022.112282.

51. Y.J. Zhang, Y.J. Liu, J. Wang, T. Zhang, State-of-health estimation for lithium-ion batteries by combining model-based incremental capacity analysis with support vector regression, Energy, 239 (2022) 342-359 DOI: 10.1016/j.energy.2021.121986.

52. N.K. Yang, Z.Y. Song, H. Hofmann, J. Sun, Robust State of Health estimation of lithium-ion batteries

using convolutional neural network and random forest, Journal Of Energy Storage, 48 (2022) 487-503 DOI: 10.1016/j.est.2021.103857.

53. G. Ma, S. Xu, T. Yang, Z. Du, L. Zhu, H. Ding, Y. Yuan, A Transfer Learning-Based Method for Personalized State of Health Estimation of Lithium-Ion Batteries, IEEE Trans Neural Netw Learn Syst, 44 (2022) 256-274 DOI: 10.1109/TNNLS.2022.3176925.

54. Y.B. Che, Y.S. Liu, Z. Cheng, J.A. Zhang, SOC and SOH Identification Method of Li-Ion Battery Based on SWPSO-DRNN, Ieee Journal Of Emerging And Selected Topics In Power Electronics, 9 (2021) 4050-4061 DOI: 10.1109/Jestpe.2020.3004972.

55. J.C. Chen, T.L. Chen, W.J. Liu, C.C. Cheng, M.G. Li, Combining empirical mode decomposition and deep recurrent neural networks for predictive maintenance of lithium-ion battery, Advanced Engineering Informatics, 50 (2021) 1147-1165 DOI: 10.1016/j.aei.2021.101405.

56. B. Zraibi, C. Okar, H.C. Chaoui, M. Mansouri, Remaining Useful Life Assessment for Lithium-Ion Batteries Using CNN-LSTM-DNN Hybrid Method, IEEE Transactions on Vehicular Technology, 70 (2021) 4252-4261 DOI: 10.1109/tvt.2021.3071622.

57. P.H. Li, Z.J. Zhang, Q.Y. Xiong, B.C. Ding, J. Hou, D.C. Luo, Y.J. Rong, S.Y. Li, State-of-health estimation and remaining useful life prediction for the lithium-ion battery based on a variant long short term memory neural network, Journal of Power Sources, 459 (2020) 264-285 DOI: 10.1016/j.jpowsour.2020.228069.

58. L. Ren, J.B. Dong, X.K. Wang, Z.H. Meng, L. Zhao, M.J. Deen, A Data-Driven Auto-CNN-LSTM Prediction Model for Lithium-Ion Battery Remaining Useful Life, IEEE Transactions on Industrial Informatics, 17 (2021) 3478-3487 DOI: 10.1109/Tii.2020.3008223.

59. X. Shu, J.W. Shen, G. Li, Y.J. Zhang, Z. Chen, Y.G. Liu, A Flexible State-of-Health Prediction Scheme for Lithium-Ion Battery Packs With Long Short-Term Memory Network and Transfer Learning, IEEE Transactions on Transportation

Electrification, 7 (2021) 2238-2248 DOI: 10.1109/Tte.2021.3074638.

60. Y.D. Gong, X.Y. Zhang, D.Z. Gao, H. Li, L.S. Yan, J. Peng, Z.W. Huang, State-of-health estimation of lithium-ion batteries based on improved long short-term memory algorithm, Journal Of Energy Storage, 53 (2022) 5784-5806 DOI: 10.1016/j.est.2022.105046.

61. F.K. Wang, Z.E. Amogne, J.H. Chou, C. Tseng, Online remaining useful life prediction of lithium-ion batteries using bidirectional long short-term memory with attention mechanism, Energy, 254 (2022) 685-698 DOI: 10.1016/j.energy.2022.124344.

62. Y. Ma, C. Shan, J.W. Gao, H. Chen, A novel method for state of health estimation of lithium-ion batteries based on improved LSTM and health indicators extraction, Energy, 251 (2022) 2561-2577 DOI: 10.1016/j.energy.2022.123973.

63. F. Heinrich, M. Pruckner, Virtual experiments for battery state of health estimation based on neural networks and in-vehicle data, Journal Of Energy Storage, 48 (2022) 1568-1589 DOI: 10.1016/j.est.2021.103856.

64. G. Cheng, X.Z. Wang, Y.R. He, Remaining useful life and state of health prediction for lithium batteries based on empirical mode decomposition and a long and short memory neural network, Energy, 232 (2021) 1364-1378 DOI: 10.1016/j.energy.2021.121022.

65. B. Zraibi, C. Okar, H. Chaoui, M. Mansouri, Remaining Useful Life Assessment for Lithium-Ion Batteries Using CNN-LSTM-DNN Hybrid Method, IEEE Transactions on Vehicular Technology, 70 (2021) 4252-4261 DOI: 10.1109/tvt.2021.3071622.

66. Y. Toughzaoui, S.B. Toosi, H. Chaoui, H. Louahlia, R. Petrone, S. Le Masson, H. Gualous, State of health estimation and remaining useful life assessment of lithium-ion batteries: A comparative study, Journal Of Energy Storage, 51 (2022) 958-975 DOI: 10.1016/j.est.2022.104520.

67. N.K. Yang, Z.Y. Song, H. Hofmann, J. Sun, Robust State of Health estimation of lithium-ion batteries using convolutional neural network and random forest, Journal Of

Energy Storage, 48 (2022) 647-659 DOI: 10.1016/j.est.2021.103857.

68. B.Y. Liu, X.P. Tang, F.R. Gao, Joint estimation of battery state-of-charge and state-of-health based on a simplified pseudo-two-dimensional model, Electrochimica Acta, 344 (2020) 412-428 DOI: 10.1016/j.electacta.2020.136098.